Arabian Journal of Chemistry (2021) **14**, 103030

King Saud University

Arabian Journal of Chemistry

www.ksu.edu.sa
www.sciencedirect.com

ORIGINAL ARTICLE

In-situ activation of NiMo catalyst based on support surface-bound thiols: A green approach to catalyst sulfidation and improved activity

Abdulkadir Tanimu [a], **Saheed A. Ganiyu** [a], **Ivan Kozhevnikov** [b], **Khalid Alhooshani** [a,*]

[a] *Department of Chemistry, King Fahd University of Petroleum and Minerals, Dhahran 31261, Saudi Arabia*
[b] *Department of Chemistry, University of Liverpool, Liverpool L69 7ZD, United Kingdom*

Received 2 November 2020; accepted 17 January 2021
Available online 2 February 2021

KEYWORDS

Hydrodesulfurization;
Sulfidation;
Thiol;
Silica;
Dibenzothiophene

Abstract The sulfidation of NiMo catalyst by thermal decomposition of support surface-bound thiols to generate stoichiometric amount of H_2S has proved to be a clean and remarkable approach for catalyst activation. The role of loading of thiol groups on the formation and dispersion of MoS_2 active phase on the mesoporous silica support was further evaluated. The catalytic activity of the supported catalysts and a reference catalyst was evaluated in the hydrodesulfurization (HDS) of dibenzothiophene. The soft acid-soft base interaction between Mo metal and thiol groups enhanced proportionately the metal's dispersion on the thiol containing support. The thermal decomposition of thiols to generate H_2S result in slow and uniform sulfidation of the NiMo to form the NiMoS catalyst. This approach of *in-situ* generation of H_2S for sulfidation provides a promising green method of activating the HDS catalysts without direct use of H_2S.

1. Introduction

There is an increasing effort to improve the activity and selectivity of hydrodesulfurization (HDS) catalysts due to the strict environmental regulations limiting the amount of sulfur in transportation fuel (Chandra Srivastava, 2012; Ganiyu et al., 2017b; Ganiyu and Alhooshani, 2019; Tanimu et al., 2019a). The activity of HDS catalysts depends mainly on the nature of the active metals, their support (in the case of supported catalysts) and the synthesis strategy adopted. A recent review article by (Tanimu and Alhooshani, 2019) has discussed the recent progress in the HDS catalyst design and development. The synthesis strategy appears to be most effective when focused on the choice of active metals and catalyst support modification. To put it simply, the synthesis strategy determines largely the prospects of the catalyst. By adopting various synthesis strategies, the formation and dispersion of active phases can be significantly enhanced, which ultimately results in high reactant conversion and product selectivity (Cao et al., 2020). By ultrasound irradiation and subsequent non-thermal plasma treatment, the phase structure, textural properties, and particularly the dispersion of the active metals of multi-walled car-

* Corresponding author.
E-mail address: hooshani@kfupm.edu.sa (K. Alhooshani).
Peer review under responsibility of King Saud University.

ELSEVIER Production and hosting by Elsevier

https://doi.org/10.1016/j.arabjc.2021.103030

bon nanotube-supported NiMoW catalyst have been significantly enhanced (Ashenaeian et al., 2018). Silicalite-1 support, prepared by 2 h sonication of the precursor solution, has good textural properties that are almost intact after impregnation with NiMo active metals (Tanimu et al., 2019b). These textural properties give the catalyst good HDS activity. Similarly, a large pore diameter Al-modified silica has been synthesized as NiMo support by anionic assisted approach; the pore diameter is more than 20 nm after impregnation of the active metals, which makes it exceptionally good HDS catalyst for sterically large sulfur compounds (Jiao et al., 2017). The synthesis strategy also involves the choice of precursors of both the active metals and support. Indeed, the formation and dispersion of active metals, the catalyst textural properties, the activation of the metal oxides and their HDS activity depend to a large extent on the type of active metal and the catalyst support precursors (Hein et al., 2017; Shan et al., 2016; Vít et al., 2014). The use of Keggin polyoxometalate (a single precursor salt containing all the active metals) has been reported as a good approach to enhance the metal dispersion due to close interaction of all metals within the polyoxometalate (Alsalme et al., 2016). Furthermore, sulfur containing alkyltrimethylammonium thiomolybdatethiotungstate cobaltate (II) has been used for *in-situ* generation of MoS_2 and WS_2 active phases in a trimetallic catalyst (Shan et al., 2016). Chelating agents such as ethylenediaminetetraacetic acid and citric acid have also been utilized to increase the formation of MoS_2 or WS_2 active phases by retarding the reduction and sulfidation of the Co-promoted Ni and Co via complex formation (Badoga et al., 2014, 2012). The approach adopted to activate the HDS catalyst to form the active MoS_2 or WS_2 phase may also have significant effect on the number of active sites formed, the active phase dispersion and the HDS activity of the catalyst (Tanimu and Alhooshani, 2019). The generally adopted technique of activation of HDS catalysts is the reduction of the active metal oxides in the flow of H_2 and subsequent sulfidation using H_2S gas or solution of CS_2. However, new techniques that exempt the direct use of these poisonous chemicals are continuously being realized and slowly getting adopted. The thermal decomposition of thiosalts such as tetraalkylammoniumthiotungstate and alkyltrimethylammoniumthiomolybdate thiotungstate-cobaltate (II) in H_2 or Ar gas has been reported as an effective approach for the synthesis of bulk MoS_2 and/or WS_2 catalysts (Espinoza-Armenta et al., 2014). A traditional wet chemistry synthesis of high density ultrasmall monolayer MoS_2 as bulk HDS catalyst has been performed by one-pot reaction of Ni $(acac)_2$/$Co(acac)_3$, $Mo(CO)_6$ and sulfur in oleylamine at 300 °C for 2 h. By using sulfur element, this approach eliminates the direct use of H_2S or CS_2 in the formation of MoS_2 active phases and the resultant catalyst has extraordinary performance (Guo et al., 2018). An *in-situ* generation of NiS and MoS_2 nanoparticles supported on graphene aerosol based on the hydrothermal synthesis of metal thiosalts solution and graphene support gives a promising HDS catalyst with a high dispersion of the active metals (Lonkar et al., 2018). Inspired by these new approaches of HDS catalyst activation, we designed a thiol containing mesoporous silica as support for NiMo catalyst in which the thiols are used as the source of H_2S for the *in-situ* sulfidation process. The thiols that are attached to the mesoporous silica support aid the dispersion of the NiMo metals via soft acid-soft base interaction. In addition, when the catalyst is heated at 500 °C, the thiols slowly decompose to release H_2S, which react with the reduced Mo to form MoS_2, the active form of the catalyst. By this approach, the direct use of highly toxic H_2S is successfully eliminated, thus making the new approach environmentally friendly and the catalyst synthesis step also became shorten. This advancement in HDS catalyst activation is compared with the general activation approach and it is demonstrated that both metal dispersion and HDS activity are greatly improved via the direct activation approach.

2. Experimental

2.1. Synthesis of thiol-functionalized silica supports

Three sets of thiol-functionalized silica supports (1RSH, 2RSH and 5RSH), each containing 1 wt%, 2 wt% and 5 wt% thiol, were prepared by addition of 0.491 g, 0.982 g and 2.455 g, respectively, of (3-mercaptopropyl)trimethoxysilane to an already stirred sol solution containing 2 g of Pluronic P123, 10.3 mL concentrated HCl, 65 mL deionized water and 4.25 mL TEOS. The solutions were further stirred for 12 h at 30 °C before transferring each solution into a Teflon-lined autoclave for hydrothermal synthesis at 90 °C for 24 h. The white powder of thiol-functionalized silica was obtained after centrifugation and drying in an oven at 100 °C overnight.

2.2. Impregnation of Ni and Mo into support framework

The catalysts were prepared by impregnation of 3 wt% Ni and 10 wt% Mo on the thiol-functionalized silica supports. Typically, 1 g of each of 1RSH, 2RSH and 5RSH silica supports was dispersed in 0.1272 g of nickel(II) acetate tetrahydrate and 0.2224 g of ammonium molybdate tetrahydrate in deionized water. The solution was stirred continuously to near dry, then subjected to drying under ambient conditions. The air-dried samples were further dried in an oven at 100 °C for 12 h. The resultant catalyst oxides (1RSH-NM, 2RSH-NM and 5RSH-NM) were later subjected to *in-situ* activation. During the dispersion of 5RSH silica support in deionized water, the support was noticed to demonstrate some hydrophobicity due to the concentration of thiol group on the silica surface and therefore did not mix efficiently with the deionized water and the metal precursors at the early stage of stirring. Thus, another 1.0 g portion of 5RSH support was further dispersed in ethanol solution containing dissolved 0.1272 g of nickel (II) acetate tetrahydrate, and a concentrated solution of 0.2224 g of ammonium molybdate tetrahydrate was subsequently added to the mixture dropwise to ensure homogeneity of the system. The formed catalyst oxide, N-5RSH-M, was also subjected to the *in-situ* activation. For the purpose of comparison, an SBA-15-NiMo catalyst (reference) with equal loading of Ni and Mo as the RSH-NM series was also prepared and activated by the general sulfidation approach of catalyst oxide reduction under the flow of 10% H_2/He and sulfidation under the flow of CS_2 solution following our previously reported method (Ganiyu et al., 2017a).

2.3. In-situ activation of the thiol-functionalized silica supported NiMo catalysts

The thiol-functionalized silica supported catalyst oxides (1RSH-NM, 2RSH-NM, 5RSH-NM and N-5RSH-M) were activated in a tubular furnace under the flow of 10% H_2/He gas at flow rate of 50 mL/min. The furnace temperature was initially set at 40 °C, then raised to 400 °C at ramping of 2 °C/min for 2 h, and in this stage, the catalyst oxide was expected to be completely reduced. Later, the temperature was raised to 500 °C (thiol decomposition temperature to form H_2S) at ramping of 5 °C/min for another 2 h after which the temperature was brought down to 40 °C for cooling at the rate of 5 °C/min. The activated catalysts were characterized accordingly and pelletized to 300–500 μm size.

2.4. Characterization of supports and catalysts

The catalyst supports and the activated catalysts were characterized using the Micromeritics ASAP 2020 to analyze their surface area and porosity based on the adsorption-desorption isotherms technique. The analysis involves sample degassing at 250 °C for 3 h under continuous flow of N_2 gas. The X-ray diffractometer, Rigaku Ultima IV, was used to measure the X-ray diffraction pattern of the activated catalysts by scanning with radiation of 40 kV and 40 mA at a speed of 3°/min in the range of 5–90° 2θ. Thermogravimetric analysis of the catalysts was carried out on SDT Q600 V20.9 instrument, by scanning from 25 °C to 700 °C at the rate of 10 °C/min under the flow of nitrogen. The FTIR spectra of catalyst supports and the activated catalysts were recorded using a Thermo Scientific Nicolet 6700 FTIR spectrometer. Typically, a 100:1 mixture of KBr and the sample was pelletized, then inserted into a sample holder which was directed to the IR source before commencing the analysis. The stacking degree and crystallite length of the MoS_2 active phase in the activated catalysts were determined from the transmission electron microscope (TEM) images, which were recorded on a JEOL-JEM-2100 operated at 200 kV. The chemical states and chemical environment of the activated catalysts were determined (under high vacuum condition) by X-ray photoelectron spectroscopy (XPS) using PHI 5000 Versa Probe II, ULVAC-PHI Inc. spectroscope. The catalysts were pelletized into an approximately 1 mm diameter disc, then attached to the sample holder and inserted into the XPS machine. The obtained XPS spectra were analyzed using the Avantage software.

2.5. Catalyst activity studies

The catalytic activity of the activated catalysts (in the pelletized form) was studied in a high-pressure Parr 4590 Micro Bench Top Reactor operated at 350 °C reaction temperature, a H_2 pressure of 5 MPa and 100 rpm stirring rate. An approximate amount of 25 mg catalyst was inserted into a 25 mL reactor vessel containing 15 mL of model fuel, which included of 1000 ppm DBT in dodecane. The reaction was monitored for 4 h after the system conditions (temperature and pressure) had been stabilized, and sampling of the model fuel was carried out at an hour interval. The sampled model fuel was analyzed for the amount of reactant and product using the gas chromatography mass spectrometer (GC–MS) technique.

3. Results and discussion

3.1. Characterization results

3.1.1. Fourier transform infrared (FTIR) spectroscopy

Functional groups that are present in both the thiol-functionalized silica supports and the activated catalysts were analyzed from the recorded FTIR spectra presented in Fig. 1 **(a)**. The spectra of pure SBA-15 silica support and thiol-functionalized silica supports show peaks that are characteristic of silica support. The peak at 3500 cm^{-1} is assigned to the O—H stretching adsorption band due to both SiO—H and HO—H functionalities, while the peaks at 1050 cm^{-1} and 750 cm^{-1} are assigned to the Si—O—Si and Si—OH stretching vibrations, respectively. Furthermore, the thiol-functionalized silica supports show an additional weak peak at 2563 cm^{-1}; the intensity of the peak increases in the higher weight percent thiol-functionalized silica (Fig. 1**(b)**). This peak, which is assigned to the —SH stretching vibration, confirmed the functionalization of SBA-15 support with the thiol group. After activation of the catalysts, the thiol peak disappears completely (Fig. 1**(c)**), which indicates the decomposition of —SH structure in the support and its possible conversion to H_2S at the activation temperature of 500 °C as reported by (Moldoveanu, 2010). The *in-situ* generated H_2S provides the direct supply of H_2S gas or CS_2 solution into tubular furnace, thus resulting in greener activation process. The scheme of the activation process is presented in Fig. 2.

3.1.2. X-ray diffraction (XRD)

The XRD pattern of the activated catalysts is presented in Fig. 3**(a)**. Interestingly, all the catalysts show a broad peak at 24.5°, which is a typical diffraction pattern observed in amorphous silica (Velmurugan et al., 2015). The diffraction peaks of the metal oxides or the corresponding sulfides were not observed in the XRD pattern of the activated catalysts, which may imply good dispersion of the catalyst on the silica support and successful conversion of the metal oxides to their sulfides. Recent study has shown that the thiol group enhanced both dispersion and ease of the reducibility of the catalysts (La Parola et al., 2012).

3.1.3. TGA analysis

The thermal analysis of the catalysts was carried out to have some insight into the decomposition temperature of the grafted thiols, which will guide the choice of catalyst activation temperature. The TGA results (Fig. 3**(b)**) of all the catalysts show a slight weight reduction (from 100 to 96%) between 80 and 100 °C which is due to evaporation of the volatile components. Thereafter, the 1RSH-NM and 2RSH-NM show a sharp decrease in weight percent, from 94 to 60%, between the temperature range of 280–500 °C, and this is ascribed to the decomposition of surface grafted thiols of the catalysts. The 5RSH-NM and N-5RSH-M catalysts show a gradual multistep decrease in the weight percent from the 280–500 °C, and this may point to the high density of the thiol groups in these catalysts that is responsible for the gradual and multistep decomposition. There was no further decrease in catalyst weight after the 500 °C, which implies that total decomposition of grafted thiols occurred at 500 °C. Therefore, the catalysts

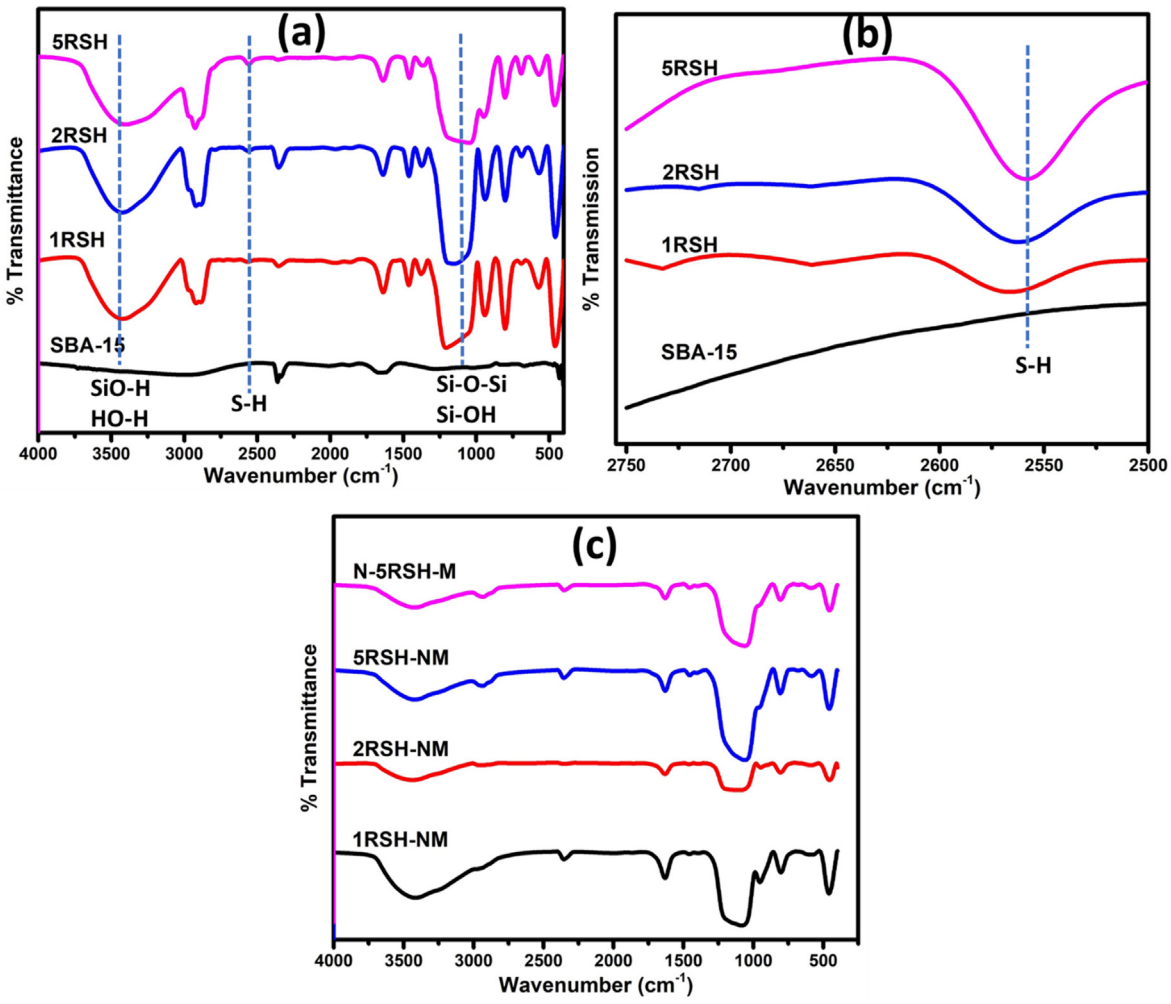

Fig. 1 FTIR spectra of: (a) SBA-15 and thiol-functionalized SBA-15; (b) magnified form of (a) showing the absorption band due to thiol group; and (c) activated catalysts.

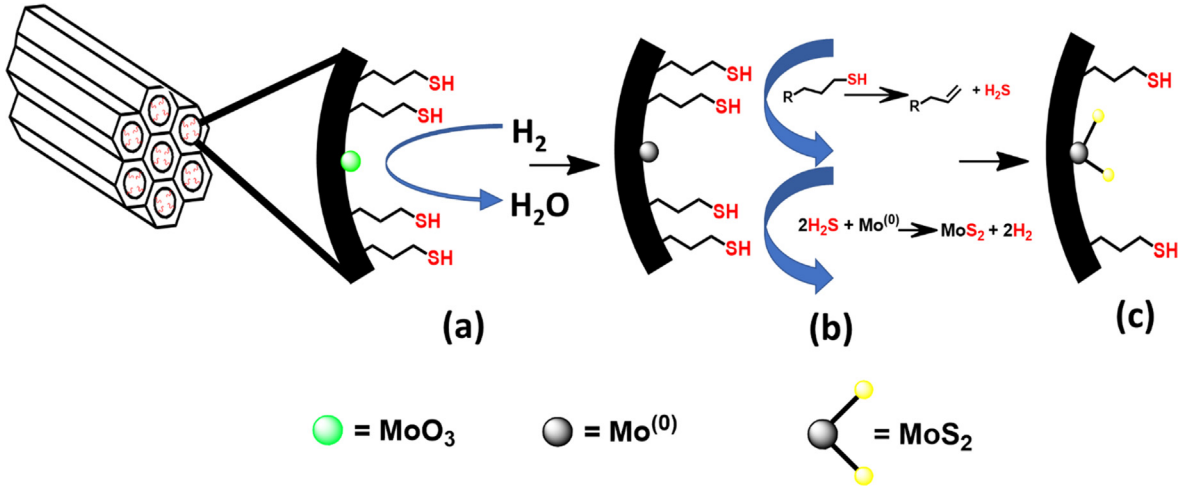

Fig. 2 Scheme for the activation of thiol-functionalized SBA-15 supported NiMo catalyst: (a) reduction of MoO_3 at 400 °C; (b) decomposition of thiol at 500 °C to release H_2S; (c) formation of MoS_2 supported on Silica.

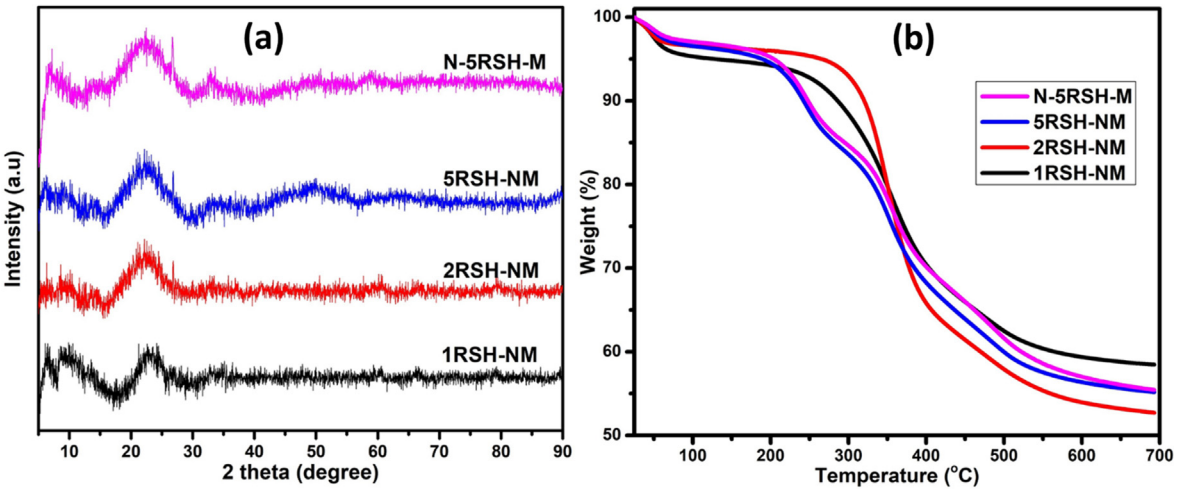

Fig. 3 (a) Wide-angle XRD and (b) TGA of the activated catalysts.

activation temperature was considered to be 500 °C. The sharp decrease in weight percent of 1RSH-NM and 2RSH-NM is an indication that the amount of thiol groups in the catalysts is relatively small, therefore, the sulfidation degree of molybdenum will be relatively lower than that of 5RSH-NM and N-5RSH-M catalysts.

3.1.4. Surface area and porosity

The surface area and pore size/pore volume of the thiol-functionalized silica supports and the activated catalysts, which were calculated based on the Brunauer, Emmett, and Teller (BET) approach and Barrett, Joyner, and Halenda (BJH) method, respectively, are summarized in Table 1. It was observed that both the BET surface area and the mesopore area of the supports decrease as the loading of thiol group is increased in the support framework. Similarly, the pore volume and pore size of the support decrease following the increase in the loading of thiol group on the silica (Fig. SI-1). The decrease in surface area and porosity is attributed to the thiol groups that were incorporated on the surface of the silica support. After loading Ni and Mo active metals and their activation to form the MoS_2 active phase, the BET surface area of the catalysts showed significant increase whereas the mesopore surface area decreased. In addition, the pore volume and pore size of the catalysts also decreased when compared to their respective silica supports. This implies that the thiol groups that were hitherto on the surface of the silica support had been removed by decomposition, thus resulting in the increased BET surface area. However, the loading of Ni and Mo active metals led to a decrease in the mesopore surface area and the pore size and pore volume of the catalysts as depicted by the N_2 adsorption-desorption isotherms of the supports and catalysts shown in Fig. 4**(a) and (b),** respectively.

The 5RSH-NM and N-5RSH-M catalysts, which were prepared using the same catalyst support but by different preparation method, showed some difference in their textural properties. It was observed that the N-5RSH-M catalyst has larger surface area and total pore volume than the 5RSH-NM and this is related to the effective mixing of the metal precursors with the thiol-functionalized silica support in the ethanol-water mixed solvent during the preparation of N-5RSH-M catalyst.

3.1.5. Transmission electron microscopy (TEM)

The effect of amount of thiol groups grafted onto the silica support on the formation and dispersion of MoS_2 active phase can be further evaluated from the TEM images of the activated catalysts. The representative TEM images (Fig. 5) depict the catalyst dispersion on the various supports after activation. All the catalysts show good degree of dispersion as evidenced from the average particle sizes of the catalysts, which is in agreement with the XRD result. In addition, the stacking length and stacking degree of the MoS_2 crystallites presented in Table 2 show that the 5RSH-NM and N-5RSH-M, with

Table 1 Textural properties of supports and catalysts.

Supports and catalysts	BET Surface area (m^2/g)	Mesopore surface area (m^2/g)	Total pore volume (cm^3/g)	Average pore size (nm)
1RSH	521	448	0.65	5.2
2RSH	256	381	0.42	5.1
5RSH	242	237	0.31	4.2
1RSH-NM	531	348	0.48	5.2
2RSH-NM	425	246	0.27	3.9
5RSH-NM	273	146	0.13	3.5
N-5RSH-M	299	166	0.15	3.4

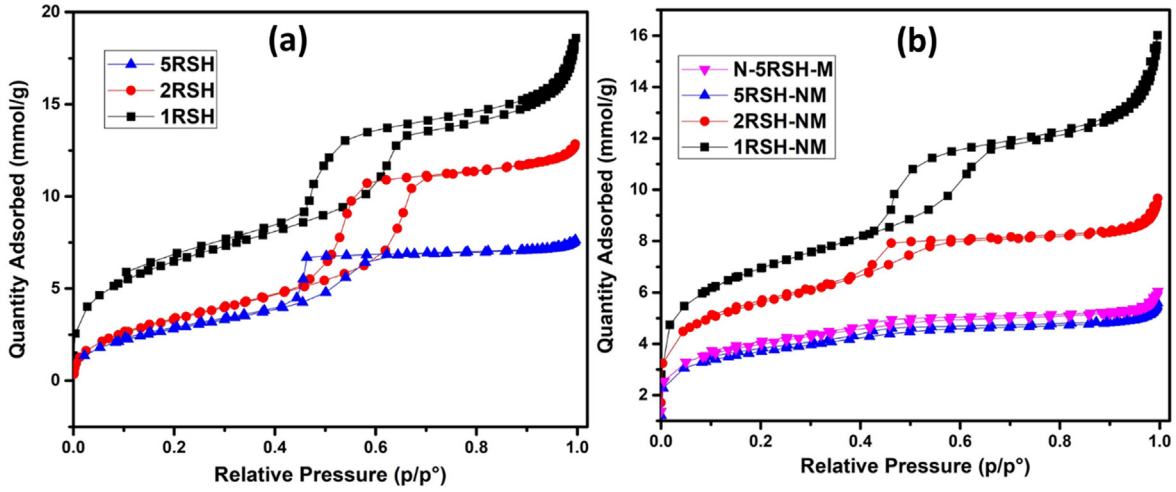

Fig. 4 N_2 adsorption–desorption isotherms of (a) thiol functionalized SBA-15 supports and (b) activated catalysts.

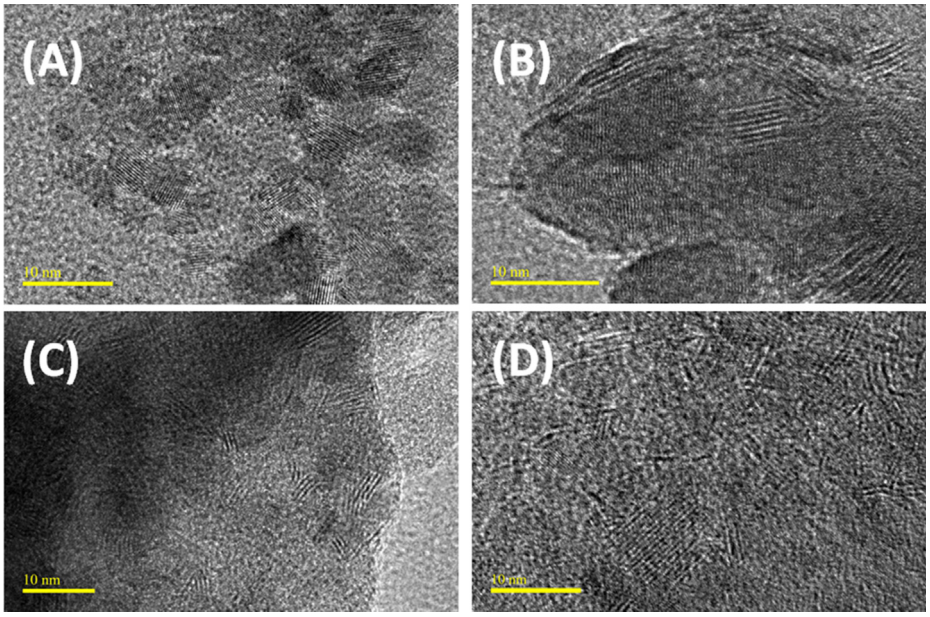

Fig. 5 TEM images of: (a) 1RSH-NM, (b) 2RSH-NM, (c) 5RSH-NM, and (d) N-5RSH-M catalysts.

Table 2 Crystallites length and stacking degree of MoS_2 in the sulfided catalysts.

Catalysts	Length distribution (nm)	Average length (nm)	Stacking distribution	Average stacking
1RSH-NM	8.2–10.6	10.3	7–10	8
2RSH-NM	7.5–11.2	10.1	6–10	9
5RSH-NM	4.2–9.8	6.3	4–8	7
N-5RSH-M	2.3–10.0	5.6	4–10	6
Reference	4.5–8.6	6.8	5–9	7

the smallest stacking length, possessed larger amount of MoS_2 active phase according to the rim-edge model (Liang et al., 2018). The N-5RSH-M catalyst shows slightly smaller stacking length, thus is likely to contain slightly larger amount of MoS_2 active phase than the 5RSH-NM, and this may be related to the slightly larger surface area of N-5RSH-M catalyst. The SBA-15-NiMo reference catalyst has stacking length and stacking degree that are within the range of those of 5RSH-NM and N-5RSH-M.

3.1.6. X-ray photoelectron spectroscopy (XPS)

The XPS analysis of the sulfided catalysts was carried out to evaluate the chemical states of the elements present in the cat-

alysts. Typically, the XPS spectrum is deconvoluted in order to account quantitatively for the chemical states present in a sample. After deconvolution, two forms of carbon were noticed in the catalysts (Fig. SI-1): carbide carbon (C1s at 282.9 eV) and graphitic carbon (C1s at 284.3 eV). An additional carbon peak at 285.6 eV was observed in the 1RSH-NM catalyst; this peak is assigned to the graphene oxide carbon which implies that there exist some C—O/C═O carbon in 1RSH-NM catalyst (Morimoto et al., 2016). It was noticed that the carbides in the RSH-NM catalysts increase as the ratio of thiol group increases (Table S-1), and this is related to the thiol group precursor, which contains the propyl group as source of carbon. Previous studies have proved that carbon, especially carbides, are good stabilizers of the transition metal sulfide catalysts, hence enhance their HDS activity (Kelty et al., 2007). Similarly, five peaks of Mo were observed in the deconvoluted spectra of Mo (Fig. 6). The peaks: Mo($3d_{5/2}$) (229.1 eV) and Mo3d($3d_{3/2}$) (232.3 eV) correspond to the doublet peaks of Mo^{4+} chemical state, and Mo3d($3d_{5/2}$) (232.8 eV) and Mo3d ($3d_{3/2}$) (235.8 eV) correspond to the doublet peaks of Mo^{6+} chemical state. The fifth peak observed around 226.4 eV is due to contribution of sulfur 2 s line. The Mo^{4+} is considered as the active form of Mo in the activated catalyst, and from Table S-1, it was observed that the percent of Mo^{4+} increases with thiol group increase (as observed by the TEM), except in the case of 5RSH-NM and N-5RSH-M where both catalysts have nearly the same percent of the Mo^{4+} active phase.

However, unlike the TEM results where the N-5RSH-M shows slightly larger amount of MoS_2 active phase, the XPS results imply that 5RSH-NM has slightly more MoS_2 crystallites. Therefore, it may be concluded that the preparation method of the 5RSH-NM and N-5RSH-M catalysts did not significantly affect the active phase formation of the catalysts although it does affect the textural properties of the catalysts. The sulfidation degree of the catalysts, calculated as the ratio of Mo^{4+} (MoS_2) to the sum of Mo^{4+} (MoS_2), Mo^{5+} (Mo_xS_y), and Mo^{6+} (MoO_3) (Gao et al., 2018), was 34.7%, 38.8%, 62.2% and 60.9% for the 1RSH-NM, 2RSH-NM, 5RSH-NM and N-5RSH-M catalysts respectively. Although the sulfidation degree is less than 80%, which is typical of sulfidation processes that do not apply H_2S directly (Texier et al., 2004), the green approach still offers a competitive advantage in terms of safety of operation.

The Ni XPS spectra (Fig. SI-2) also depict two Ni chemical states: Ni2p (854.9 eV) and Ni2p (860.1 eV); these chemical states correspond to the catalytically active NiMoS phase according to Zhou et al. (Zhou et al., 2018). The percent of NiMoS phase in the catalysts (Table S-1) followed the trend: 1RSH-NM < 2RSH-NM < 5RSH-NM ~ N-5RSH-M, which like in the case of Mo^{4+}, implies that the 5RSH-NM or N-

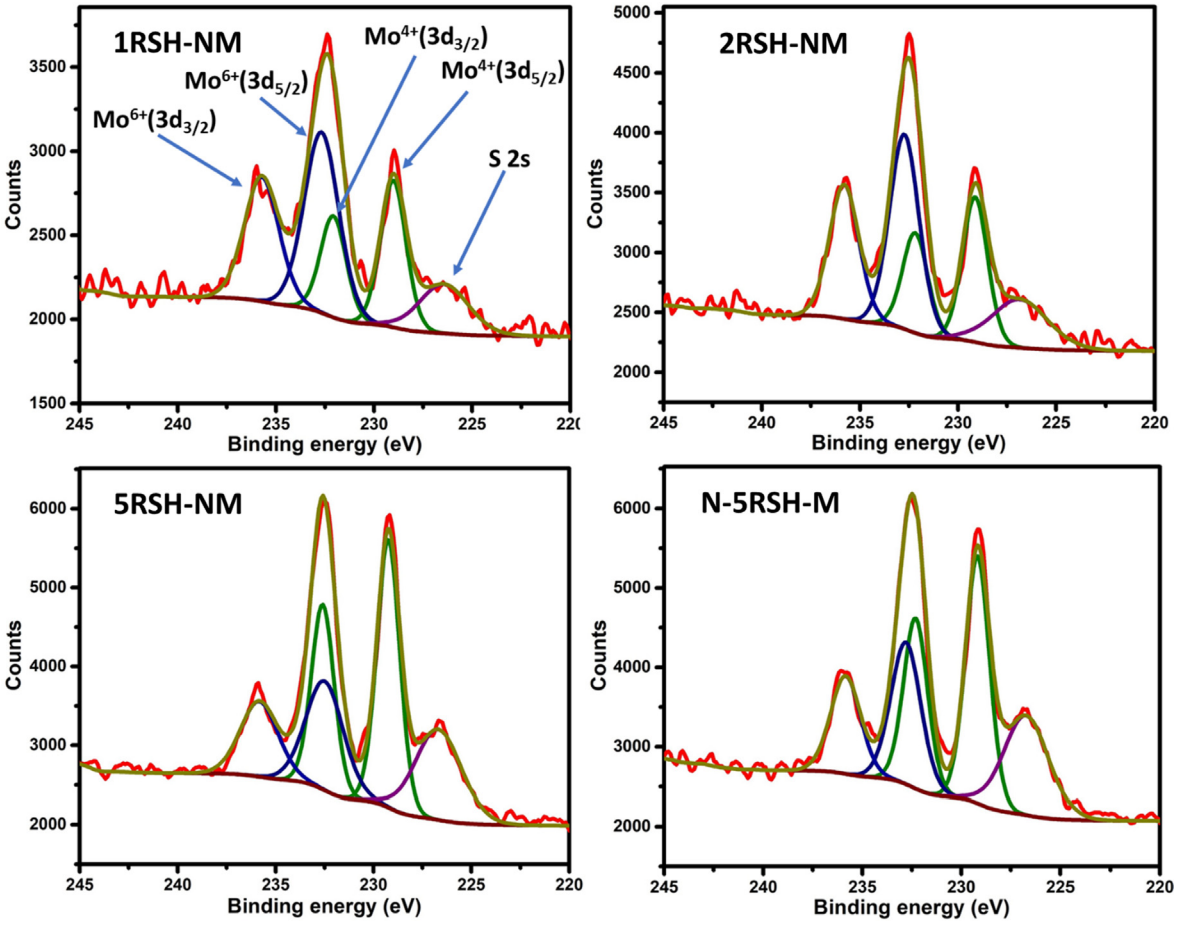

Fig. 6 XPS spectra of sulfided catalysts showing the peaks of Mo3d chemical states.

5RSH-M catalyst is likely to be the most active catalyst for the HDS reaction.

3.2. Catalyst activity and selectivity studies

The activity of the catalysts was studied based on the percentage of DBT removal over a reaction time of 4 h. The plot of HDS activity for the catalysts (Fig. 7) shows that the new activation strategy for the catalysts does enhance the activity of the catalysts in addition to offering a safer activation process that is free from the direct use of H_2S. Table S-2 gives the percentage of DBT removal over the reaction time of 4 h for the catalysts studied. It was observed that the reference catalyst had a conversion of 35% in 1 h reaction time, which was the lowest conversion among the catalysts studied. The activity (conversion) sequence of the catalysts after 1 h of reaction is: N-5RSH-M (52.0%) > 5RSH-NM (47.8%) > 2RSH-NM (46.5%) > 1RSH-NM (39.9%) > reference (35.4%). The observed trend agrees with the results of catalyst characterization, which shows that the formation of active metals and their dispersion on the silica support is strongly influenced by the amount of thiol groups on the surface of the support as previously reported by Parola et al. (La Parola et al., 2012).

Furthermore, during the activation, carbon was formed from the propyl group attached at alpha-position to the —SH group and this carbon played a positive role in the HDS activity of the catalysts. The activity of the catalysts continued to increase with the reaction time up to 4 h. However, the conversion trend changed over the reaction time. After 2 h, the reference catalyst outperformed 1RSH-NM. At 3 and 4 h, the reference catalyst performed better than all the catalysts under study except for N-5RSH-M, which had a conversion of 91%. This implies that the 1RSH-NM and 2RSH-NM catalysts are likely to deactivate faster than the reference catalyst (see the first order rate constants at 1 h and 4 h reaction time in Table S-3). A slight decrease in the rate constant for the N-5RSH-M catalyst over the reaction time of 4 h is typical of HDS reactions where the reaction rate decreases slightly with time due to gradual catalyst deactivation. Overall, it may be concluded that within the studied reaction time, the N-5RSH-M catalyst stands out to be the best catalyst after 4 h reaction time. The better performance of the N-5RSH-M catalyst may be attributed to the larger surface area, increased amount of active phase and better dispersion as can be suggested from the BET, TEM and XPS analysis. The selectivity studies of the catalysts were performed using the product distribution and first order rate constants shown in Table S-3. As presented in the table, all the catalysts formed only biphenyl as the product except for the reference catalyst. This means that the HDS reaction occurs via the most preferred direct desulfurization pathway with these catalysts except for the reference catalyst which shows little formation of cyclohexylbenzene, thus indicating that some of the HDS reaction occurred via the hydrogenation pathway.

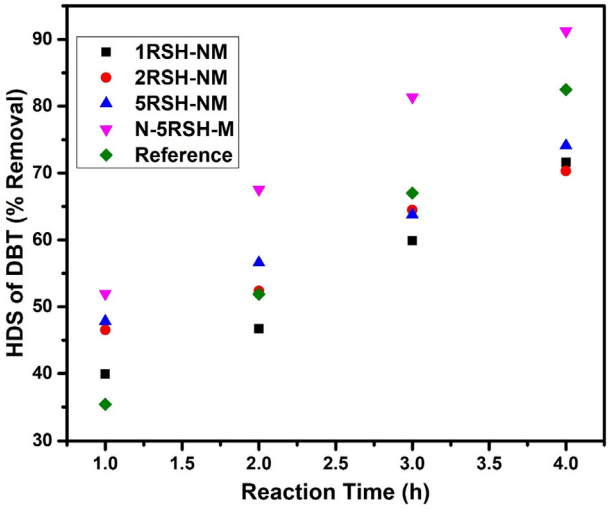

Fig. 7 HDS activity plot for synthesized catalysts and reference catalyst.

4. Conclusion

In this study, a new approach to the sulfidation of mesoporous silica-supported NiMo catalysts has been presented. This approach includes grafting thiol groups onto the surface of the silica support, followed by decomposition of the grafted thiol groups at 500 °C to slowly release H_2S, which reacts with the impregnated and reduced NiMo metals to form the active NiMoS phase. This in-situ generation of H_2S has provided a green approach for the sulfidation of silica-supported NiMo catalysts by preventing the direct use of H_2S gas. The FTIR results confirm the loading of the thiol groups and the TEM and XPS analyses show that a larger amount of better dispersed MoS_2 is formed in the 5 wt% thiol-grafted silica-supported NiMo catalyst. The textural analysis shows that the 5 wt% thiol-grafted silica-supported catalyst N-5RSH-M prepared by dispersing the catalyst support in ethanol has larger surface area than its analog 5RSH-NM that was dispersed in deionized water. The better structural properties of the N-5RSH-M catalyst result in its enhanced catalytic activity even beyond that of the silica-supported NiMo catalyst that was sulfided by the direct treatment with H_2S gas or a solution of CS_2.

Declaration of Competing Interest

The authors declare no competing interest.

Acknowledgements

The authors acknowledged the support provided by King Fahd University of Petroleum and Minerals (KFUPM) for funding this work through project No. DSR SL191003.

Appendix A. Supplementary material

Pore size distribution plot, XPS analysis table, XPS spectra of carbon C1s chemical states, XPS spectra of Ni2p chemical states, table of percent DBT removal, and table of product distribution. Supplementary data to this article can be found online at https://doi.org/10.1016/j.arabjc.2021.103030.

References

Alsalme, A., Alzaqri, N., Alsaleh, A., Siddiqui, M.R.H., Alotaibi, A., Kozhevnikova, E.F., Kozhevnikov, I.V., 2016. Efficient Ni–Mo hydrodesulfurization catalyst prepared through Keggin polyoxometalate. Appl. Catal. B Environ. 182, 102–108. https://doi.org/10.1016/J.APCATB.2015.09.018.

Ashenaeian, S., Haghighi, M., Rahemi, N., 2018. Hybrid plasma-sono-coprecipitation dispersion of NiMo nanocatalyst over functionalized multiwall carbon nanotube used in hydrodesulfurization of thiophene. Adv. Powder Technol. https://doi.org/10.1016/j.apt.2018.12.001.

Badoga, S., Dalai, A.K., Adjaye, J., Hu, Y., 2014. Combined effects of EDTA and heteroatoms (Ti, Zr, and Al) on catalytic activity of SBA-15 supported NiMo catalyst for hydrotreating of heavy gas oil. Ind. Eng. Chem. Res. 53, 2137–2156. https://doi.org/10.1021/ie400695m.

Badoga, S., Mouli, K.C., Soni, K.K., Dalai, A.K., Adjaye, J., 2012. Beneficial influence of EDTA on the structure and catalytic properties of sulfided NiMo/SBA-15 catalysts for hydrotreating of light gas oil. Appl. Catal. B Environ. 125, 67–84. https://doi.org/10.1016/j.apcatb.2012.05.015.

Cao, H., Bai, Z., Li, Y., Xiao, Z., Zhang, X., Li, G., 2020. Solvothermal Synthesis of Defect-Rich Mixed 1T–2H MoS2Nanoflowers for Enhanced Hydrodesulfurization. ACS Sustain. Chem. Eng. 8, 7343–7352. https://doi.org/10.1021/acssuschemeng.0c00736.

Chandra Srivastava, V., 2012. An evaluation of desulfurization technologies for sulfur removal from liquid fuels. RSC Adv. 2, 759. https://doi.org/10.1039/c1ra00309g.

Espinoza-Armenta, Y., Cruz-Reyes, J., Paraguay-Delgado, F., Del Valle, M., Alonso, G., Fuentes, S., Romero-Rivera, R., 2014. CoMoW sulfide nanocatalysts for the HDS of DBT from novel ammonium and alkyltrimethylammonium-thiomolybdatethiotungstate-cobaltate (II) precursors. Appl. Catal. A Gen. 486, 62–68. https://doi.org/10.1016/j.apcata.2014.08.017.

Ganiyu, S.A., Alhooshani, K., 2019. Catalytic Performance of NiMoS Supported on (Zr)SBA-15 for Hydrodesulfurization of Diesel: Insight into a One-Step Calcination and Reduction Strategy during Sulfidation. Energy Fuels 33, 3047–3056. https://doi.org/10.1021/acs.energyfuels.8b04536.

Ganiyu, S.A., Alhooshani, K., Ali, S.A., 2017a. Single-pot synthesis of Ti-SBA-15-NiMo hydrodesulfurization catalysts: Role of calcination temperature on dispersion and activity. Appl. Catal. B Environ. 203, 428–441. https://doi.org/10.1016/j.apcatb.2016.10.052.

Ganiyu, S.A., Ali, S.A., Alhooshani, K., 2017b. Simultaneous HDS of DBT and 4,6-DMDBT over single-pot Ti-SBA-15-NiMo catalysts: influence of Si/Ti ratio on the structural properties, dispersion and catalytic activity. RSC Adv. 7, 21943–21952. https://doi.org/10.1039/C7RA01806A.

Gao, Y., Han, W., Long, X., Nie, H., Li, D., 2018. Preparation of hydrodesulfurization catalysts using MoS3 nanoparticles as a precursor. Appl. Catal. B Environ. 224, 330–340. https://doi.org/10.1016/j.apcatb.2017.10.046.

Guo, K., Ding, Y., Yu, Z., 2018. One-step synthesis of ultrafine MoNiS and MoCoS monolayers as high-performance catalysts for hydrodesulfurization and hydrodenitrogenation. Appl. Catal. B Environ. 239, 433–440. https://doi.org/10.1016/J.APCATB.2018.08.041.

Hein, J., Gutiérrez, O.Y., Albersberger, S., Han, J., Jentys, A., Lercher, J.A., 2017. Towards Understanding Structure-Activity Relationships of Ni-Mo-W Sulfide Hydrotreating Catalysts. ChemCatChem 9, 629–641. https://doi.org/10.1002/cctc.201601281.

Jiao, J., Fu, J., Wei, Y., Zhao, Z., Duan, A., Xu, C., Li, J., Song, H., Zheng, P., Wang, X., Yang, Y., Liu, Y., 2017. Al-modified dendritic mesoporous silica nanospheres-supported NiMo catalysts for the hydrodesulfurization of dibenzothiophene: Efficient accessibility of active sites and suitable metal–support interaction. J. Catal. 356, 269–282. https://doi.org/10.1016/J.JCAT.2017.10.003.

Kelty, S.P., Berhault, G., Chianelli, R.R., 2007. The role of carbon in catalytically stabilized transition metal sulfides. Appl. Catal. A Gen. 322, 9–15. https://doi.org/10.1016/j.apcata.2007.01.017.

La Parola, V., Testa, M.L., Venezia, A.M., 2012. Pd and PdAu catalysts supported over 3-MPTES grafted HMS used in the HDS of thiophene. Appl. Catal. B Environ. 119–120, 248–255. https://doi.org/10.1016/j.apcatb.2012.03.007.

Liang, J., Wu, M., Wang, J., Wei, P., Sun, B., Lu, Y., Sun, D., Liu, Y., Liu, C., 2018. A new approach to construct a hydrodesulfurization catalyst from a crystalline precursor: ligand-induced self-assembly, sulfidation and hydrodesulfurization. Catal. Sci. Technol. 8, 6330–6345. https://doi.org/10.1039/C8CY02007H.

Lonkar, S.P., Pillai, V.V., Alhassan, S.M., 2018. Three-Dimensional NiS-MoS $_2$ /Graphene Heterostructured Nanohybrids as High-Performance Hydrodesulfurization Catalysts. ACS Appl. Nano Mater. 1, 3114–3123. https://doi.org/10.1021/acsanm.8b00287.

Moldoveanu, S.C., 2010. Chapter 12 Pyrolysis of Thiols and Sulfides. Tech. Instrum. Anal. Chem., https://doi.org/10.1016/S0167-9244(09)02812-1.

Morimoto, N., Kubo, T., Nishina, Y., 2016. Tailoring the Oxygen Content of Graphite and Reduced Graphene Oxide for Specific Applications. Sci. Rep. 6, 21715. https://doi.org/10.1038/srep21715.

Shan, S., Liu, H., Yue, Y., Shi, G., Bao, X., 2016. Trimetallic WMoNi diesel ultra-deep hydrodesulfurization catalysts with enhanced synergism prepared from inorganic–organic hybrid nanocrystals. J. Catal. 344, 325–333. https://doi.org/10.1016/J.JCAT.2016.09.019.

Tanimu, A., Alhooshani, K., 2019. Advanced Hydrodesulfurization Catalysts: A Review of Design and Synthesis. Energy Fuels 33, 2810–2838. https://doi.org/10.1021/acs.energyfuels.9b00354.

Tanimu, A., Ganiyu, S.A., Adamu, S., Alhooshani, K., 2019a. Synthesis, application and kinetic modeling of CeO x –Si–CoMo catalysts for the hydrodesulfurization of dibenzothiophene. React. Chem. Eng. 4, 724–737. https://doi.org/10.1039/C8RE00330K.

Tanimu, A., Ganiyu, S.A., Jillani, S.M.S., Umar, M., Adamu, S., Alhooshani, K., 2019b. Sono-Assisted Synthesis and Kinetic Modeling of Nanocrystallite Silicalite-1-NiMo Catalysts for Hydrodesulfurization of Dibenzothiophene: Role of Sonication Time on Support Mesoporosity and Catalytic Activity. Ind. Eng. Chem. Res. 58, 18550–18560. https://doi.org/10.1021/acs.iecr.9b03358.

Texier, S., Berhault, G., Pérot, G., Harlé, V., Diehl, F., 2004. Activation of alumina-supported hydrotreating catalysts by organosulfides: Comparison with H2S and effect of different solvents. J. Catal. 223, 404–418. https://doi.org/10.1016/j.jcat.2004.02.011.

Velmurugan, P., Shim, J., Lee, K.-J., Cho, M., Lim, S.-S., Seo, S.-K., Cho, K.-M., Bang, K.-S., Oh, B.-T., 2015. Extraction, characterization, and catalytic potential of amorphous silica from corn cobs by sol-gel method. J. Ind. Eng. Chem. 29, 298–303. https://doi.org/10.1016/J.JIEC.2015.04.009.

Vít, Z., Gulková, D., Kaluža, L., Boaro, M., 2014. Effect of catalyst precursor and its pretreatment on the amount of β-Pd hydride phase and HDS activity of Pd-Pt/silica-alumina. Appl. Catal. B Environ. 146, 213–220. https://doi.org/10.1016/J.APCATB.2013.02.055.

Zhou, W., Zhang, Y., Tao, X., Zhou, Y., Wei, Q., Ding, S., 2018. Effects of gallium addition to mesoporous alumina by impregnation on dibenzothiophene hydrodesulfurization performances of the corresponding NiMo supported catalysts. Fuel 228, 152–163. https://doi.org/10.1016/J.FUEL.2018.04.084.